

Radiative forcing from surface NO_x emissions: spatial and seasonal variations

R. G. Derwent · D. S. Stevenson · R. M. Doherty ·
W. J. Collins · M. G. Sanderson · C. E. Johnson

Received: 24 February 2006 / Accepted: 7 November 2007
© Springer Science + Business Media B.V. 2007

Abstract The global three-dimensional Lagrangian chemistry-transport model STOCHEM has been used to follow changes in the tropospheric distributions of methane CH₄ and ozone O₃ following the emission of pulses of the oxides of nitrogen NO_x. Month-long emission pulses of NO_x produce deficits in CH₄ mixing ratios that bring about negative radiative forcing (climate cooling) and decay away with e-folding times of 10–15 years. They also produce short-term excesses in O₃ mixing ratios that bring about positive radiative forcing (climate warming) that decay over several months to produce deficits, with their attendant negative radiative forcing (climate cooling) that decays away in step with the CH₄ deficits. Total time-integrated net radiative forcing is markedly influenced by cancellation between the negative CH₄ and long-term O₃ contributions and the positive short-term O₃ contribution to leave a small negative residual. Consequently, total net radiative forcing from NO_x emission pulses and the global warming potentials derived from them, show a strong dependence on the magnitudes, locations and seasons of the emissions. These dependences are illustrated using the Asian continent as an example and demonstrate that there is no simple robust relationship between continental-scale NO_x emissions and globally-integrated radiative forcing. We find that the magnitude of the time-integrated radiative forcing from NO_x-driven CH₄ depletion tends to approach and outweigh that from ozone enhancement, leaving net time-integrated radiative forcings and global warming potentials negative (climate cooling) in contrast to the situation for aircraft NO_x (climate warming). Control of man-made surface NO_x emissions alone may lead to positive radiative forcing (climate warming).

R. G. Derwent (✉)
rdsscientific, Newbury, Berkshire, UK
e-mail: r.derwent@btopenworld.com

D. S. Stevenson · R. M. Doherty
Institute for Atmospheric and Environmental Science, University of Edinburgh, Edinburgh, UK

W. J. Collins · M. G. Sanderson · C. E. Johnson
The Met Office, Exeter, Devon, UK

1 Introduction

Emissions of nitrogen oxides NO_x from human activities, together with those of methane CH_4 , carbon monoxide CO and organic compounds VOCs , take part in controlling the oxidizing capacity of the troposphere and hence the atmospheric lifetime of CH_4 and its global-scale build-up. The growth in NO_x emissions from human activities since pre-industrial times has also brought about an increase in the tropospheric ozone O_3 burden (Volz and Kley 1988) and is associated with a positive radiative forcing of climate. The Intergovernmental Panel on Climate Change (2001) report that the radiative forcings from the changes in atmospheric composition of methane and tropospheric ozone since pre-industrial times are the second and third most important trace gas forcings after carbon dioxide CO_2 . In addition, NO_x emissions have further impacts on climate through the formation of nitrate aerosol (Schaap et al. 2004; Liao and Seinfeld 2005) and from impacts on the carbon cycle (Schimel 1995). Despite the magnitude of these radiative forcings, NO_x emissions, in particular, and tropospheric O_3 precursor gases, in general, have not been included in the basket of trace gases within the Kyoto Protocol to the United Nations Framework Convention on Climate Change.

Policy actions on climate change need to take into account the relative magnitudes and timescales of the many radiative forcing agents, such as CO_2 , CH_4 and O_3 , and processes, such as land-use change and global aviation (IPCC 2001). A range of different climate change metrics have been proposed but here, attention will be given to two metrics in particular: radiative forcing RF and global warming potential GWP . RF is an instantaneous property of the atmosphere and has been extensively defined, reviewed and utilised by the IPCC (1990). It has been employed to quantify the impact on the transmission of radiation through the atmosphere due to changes in the trace gas distributions since pre-industrial times but takes no account of how long such changes will persist in the absence of the human activities that are driving them. The concept of the global warming potential GWP has been introduced to provide a measure of the relative importance of the different trace gases for their influence on the climate system.

The GWP of a trace gas is defined as the instantaneous mass emission of carbon dioxide that gives the same time-integrated radiative forcing as the instantaneous emission of unit mass of the trace gas when considered over a given time horizon. The radiative properties of the trace gas control the absorption of radiation per unit mass burden but the atmospheric lifetime, or more accurately the adjustment time, controls how long a given mass burden of the trace gas is retained in the atmosphere and influences the climate system. The choice of time horizon is up to the user but here we adopt a 100-year time horizon. The background to the definition and estimation of GWPs is given elsewhere (IPCC 1990; IPCC 1995; WMO 1999) and is further discussed in Godal and Fuglestedt (2002) and Shine et al. (2005a). The time-integrated radiative forcing over a given time horizon is sometimes referred to as the absolute global warming potential, AGWP . Here, we restrict our usage of the terms time-integrated radiative forcing and GWP to CH_4 and O_3 and of AGWP to the reference gas for the GWPs , namely CO_2 . It is important to note that the instantaneous emission of NO_x does not itself induce radiative forcing because NO_x is not a radiative forcing agent. However, emission pulses of NO_x induce changes in the tropospheric distributions of CH_4 and O_3 , so NO_x is an indirect greenhouse gas.

There are many questions concerning the wisdom of combining all the biogeochemical properties of the trace gases into a single climate change metric (Fuglestedt et al. 2003 and the references therein). There are questions concerning the relationship between radiative forcing and climate response and whether the same climate sensitivity parameter is

appropriate for all trace gases and radiative forcing agents (Hansen et al. 2005; Joshi et al. 2003). There are also proposals for different indices based on climate responses such as global temperature (Shine et al. 2003; 2005a). Radiative forcing indices for some agents may be location dependent (Fuglestedt et al. 1999; Berntsen et al. 2005; Naik et al. 2005; Berntsen et al. 2006). Estimates of radiative forcing are also influenced by how vertical temperature gradients, surface albedo and clouds are described in models. Here, the concern is that there is no simple robust relationship between trace gas emission and radiative forcing for some radiative forcing agents, particularly the tropospheric O₃ precursors (Shine et al. 2005b), and this contributes further to uncertainty and hesitancy on the part of policymakers.

Changes in the emissions of short-lived trace gases, such as CO and NO_x, cause changes in the oxidizing capacity of the troposphere and induce perturbations in the distributions of CH₄ and O₃ (Fuglestedt et al. 1999; Wild and Prather 2000; Derwent et al. 2001). These perturbations persist long after the change in emissions was initiated. The perturbations are dispersed and transported and may become well-mixed on the hemispheric and global scales, at least for CH₄. CH₄ perturbations decay away with time constants that are a factor of about 1.4–1.5 times longer than the atmospheric lifetime (Wild and Prather 2000). Short-lived trace gases can therefore indirectly cause radiative forcing responses that are global in character and persist over decadal time-scales. A difficulty is that the magnitudes of the CH₄ and O₃ responses appear to depend on where and when the changes in trace gas emissions were made (Berntsen et al. 2005; Naik et al. 2005). Emissions of NO_x from aircraft in the upper troposphere and lower stratosphere appear to have a much stronger effect on ozone than if the same amounts of NO_x were emitted at the surface (Fuglestedt et al. 1996; IPCC 1999). Fuglestedt et al. (1999) found a much higher sensitivity for upper tropospheric O₃ to reductions in NO_x emissions from surface sources in Asia and Australia compared with North America and Europe.

In previous studies, we have employed the global Lagrangian chemistry–climate model STOCHEM to study the radiative forcings generated by aircraft NO_x emissions (Stevenson et al. 2004) and surface sources of CO, NO_x and CH₄ (Derwent et al. 2001) and VOCs (Collins et al. 2002). In these studies, the STOCHEM model was used to follow the changes in the tropospheric distributions of methane and ozone brought about by the addition of emission pulses of the tropospheric ozone precursor gases. Here, a similar approach has been adopted to the study of the radiative forcings due to CH₄ and O₃, generated by surface NO_x emissions. Attention has been given to the spatial and seasonal variations in the emission and forcing relationships and the mechanisms that drive them.

2 Description of the climate–chemistry model STOCHEM

STOCHEM is a global Lagrangian tropospheric chemistry-transport model, originally described by Collins et al. (1997). In the work described here, an early version of the model was employed in which the atmosphere is divided into 50,000 air parcels that are mapped after each advection time-step to a 5°×5° resolution grid with 9 vertical layers up to 100 hPa. Input meteorology is provided by the Met Office numerical weather prediction models as analysis fields with a resolution of 1.25° longitude and 0.83° latitude and on 12 vertical levels, extending to 100 hPa. The advection time-step is 3 h. Turbulent mixing in the boundary layer is achieved by randomly re-assigning the vertical co-ordinates of air parcels over the depth of the planetary boundary layer height. Small-scale convective processes are treated by randomly mixing a fraction of the air parcels between the surface

and the cloud top, depending on the convective cloud top, convective cloud cover and convective precipitation rate. Air parcel advection is performed using a fourth order Runge–Kutta method with the winds bilinearly interpolated to the parcel's location in the horizontal and using cubic interpolation in the vertical.

The chemical scheme includes 70 species that take part in 174 photochemical gas and aqueous phase reactions. The chemical scheme uses a backwards Euler solver using a time step of 5 min. Wet deposition operates on all soluble species using scavenging coefficients and dry deposition follows a resistance approach. O₃ and NO_y upper boundary conditions are imposed by prescribing fluxes into the top layer of the model at 100 hPa. These fluxes were derived using vertical winds at 100 hPa together with an ozone climatology (Li and Shine 1995). NO_y influxes were fixed to those of O₃ by assuming a fixed mass ratio of N:O₃ of 1:1,000 (Murphy and Fahey 1994).

Emission fields for a wide range of man-made trace gases including CH₄, CO, NO_x and VOCs have been developed for 2000 by the International Institute for Applied Systems Analysis (IIASA) are described in detail elsewhere (Cofala et al. 2005; Dentener et al. 2005). Vegetation emissions of isoprene were set at 500 Tg year⁻¹ and lightning NO_x emissions at 5.0 Tg N year⁻¹. Aircraft emissions were based on the NASA 1992 inventory (IPCC 1999) and were set at 0.5 Tg N year⁻¹. The SO₂ and NO_x emissions from international shipping were based on EDGAR v3.2 data for 1995 (Olivier and Berdowski 2001), with an assumed growth rate of 1.5% per year between 1995 and 2000 (Dentener et al. 2005). Emissions of methane from wetlands, tundra and rice paddies were set at 260 Tg year⁻¹. Surface emissions are added on a 5°×5° grid square basis and this gives an average cell occupancy of roughly two Lagrangian cells within the boundary layer per grid square in the mid-latitudes. After each advection timestep, the surface emissions are distributed equally over all the Lagrangian cells that are within the boundary layer for a particular grid square. If there are no cells within the boundary layer for a particular grid square then the emissions are stored until a cell passes through.

3 Experiments

The transient behaviour of CH₄ and O₃ in response to emission pulses of NO_x were investigated using the global Lagrangian CTM model STOCHEM by starting the model from an initial set of trace gas mixing ratios on 1st October 1997 and using analysed wind fields to run through to 1st January 1998. At that point, two model runs were initiated. The first model run, the base case, continued on from the previous annual cycle without change until 31st December 1998. In the second model run, the transient case, the NO_x emission source was changed so that a pulse containing an additional or decreased amount of NO_x was emitted into the model during the period from 1st January to 31st January 1998. At this point, the NO_x emissions were reset to the base case value and the model run was continued until 31st December 1998. The impacts of NO_x on the composition of the model troposphere were followed by taking differences between the trace gas concentrations in the base and transient cases. Increases in mixing ratios or global burdens between the two model runs were termed 'excess' mixing ratios or burdens and decreases, 'deficits'. The application of such pulse experiments to CH₄, CO, H₂ and NO_x is described in Derwent et al. (2001) and to VOCs in Collins et al. (2002).

To estimate the overall climate forcings from surface NO_x emissions, time-integrated radiative forcings RFs were calculated for the CH₄ and O₃ perturbations over a 100-year time horizon following Derwent et al. (2001) and Wild et al. (2001). As explained in

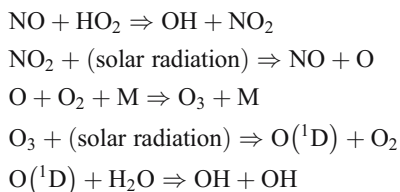
Stevenson et al. (2004), because the CH₄ perturbations are long-lived, they become well-mixed throughout the atmosphere and RF calculations are straightforward. Time-integrated CH₄ anomalies in ppb years are converted into RFs using a simple relationship between forcing and change in concentration of 0.37 mW m⁻² ppb⁻¹ (Schimel et al. 1996) and are presented in Table 4. The conversion between time-integrated ozone responses and RFs for ozone employed an off-line radiation code (Edwards and Slingo 1996) following the methods described in Stevenson et al. (1998, 2004). Full account is taken of stratospheric temperature adjustment which reduced forcings by about 22%. Long-term time-integrated ozone forcings were calculated assuming a fixed ratio of 0.23 between the long-term O₃ forcing and the CH₄ forcing, as found previously in longer time period (5 years) integrations using a closely related model version (Stevenson et al. 2004).

4 Model results

4.1 Hemispheric-scale NO_x emission pulses

In the first set of experiments, the NO_x emission pulses were applied during January 1998 at a constant areal emission density over an area of 80° longitude×40° latitude centred on North America, Europe and Asia. The total additional NO_x emission over each region was 2 Tg N during the period of the pulse. The size of the emission pulse was arbitrary and was chosen to be small enough so that the resulting NO_x emission densities were not unreasonably high, yet large enough to bring about discernible changes in mixing ratios. We later investigate the influence of the size of the pulse on the resultant forcings per unit emission.

In response to the NO_x emission pulses, systematic differences were found in trace gas mixing ratios and global burdens between the base and transient cases in each of the three experiments. The global burden of NO_x (=NO+NO₂) increased quickly during January in the transient case over and above that in the base case and the excess decayed away quickly with an e-folding time of 2.5 days after the pulse had finished. Immediate increases were observed in the OH and O₃ mixing ratios through the following reactions:



Excess OH and O₃ burdens built up in the regions where the NO_x emission densities had been perturbed and in the areas immediately downwind of them and decayed away quickly during February. The increased OH burdens in the transient case led to increased OH+CH₄ reaction fluxes and hence to decreased CH₄ burdens. The deficit in the CH₄ burdens steadily built up and stabilized both in magnitude and spatial distribution during the first 4–6 months and then began to decay away steadily during the rest of the year. In our previous studies, we have shown that the deficits in the global CH₄ burdens decay away with time constants of between 10–15 years, the CH₄ adjustment time constant (Derwent et al. 2001) and taken to be 11.5 years on the basis of the 5-year model experiments described by Stevenson et al. (2004). Excess O₃ burdens reached a peak during January and then

decayed away rapidly during March and April. The decay continued during May and June, taking the excess ozone below zero, (not shown in Fig. 1), producing an O_3 deficit in the transient case. This deficit stabilized during the remainder of the first year and began decaying away slowly. It was associated strongly with the CH_4 deficit and, as in previous studies, it decayed away with the same time constant as the CH_4 deficit (Stevenson et al. 2004). This long-term behaviour is the so-called “primary mode” as described by Wild and Prather (2000).

Time-integrated perturbations to the global burdens of CH_4 and O_3 were calculated from the differences in the respective burdens between the transient and model experiments. They were comprised of two contributions: the first was from the initial short-term phase that was estimated from the model results in the first year; the second was from the long-term phase that was obtained by extrapolating the model results from the end of December 1998 onwards using the methane adjustment time as described in Stevenson et al. (2004). In all cases, a CH_4 adjustment time constant of 11.5 years was assumed (Stevenson et al. 2004). For the time-integrated perturbations to the CH_4 burdens, both contributions were negative and the second term dominated over the first by at least an order of magnitude and so the former term was not considered separately from the latter. For the time-integrated perturbations to the O_3 burdens, the initial short-term and long-term contributions were of opposite sign because the first term was positive, being dominated by the initial NO_x -driven perturbation, and the second term was negative, being dominated by the CH_4 -driven O_3 perturbation. Although the magnitude of the monthly values of the CH_4 -driven perturbation were tiny compared with the initial NO_x -driven perturbation, their persistence on the decadal timescale meant that they could not be neglected on a time-integrated basis. All perturbations were scaled assuming complete linearity and normalized to a NO_x emission pulse of 1 Tg NO_2 .

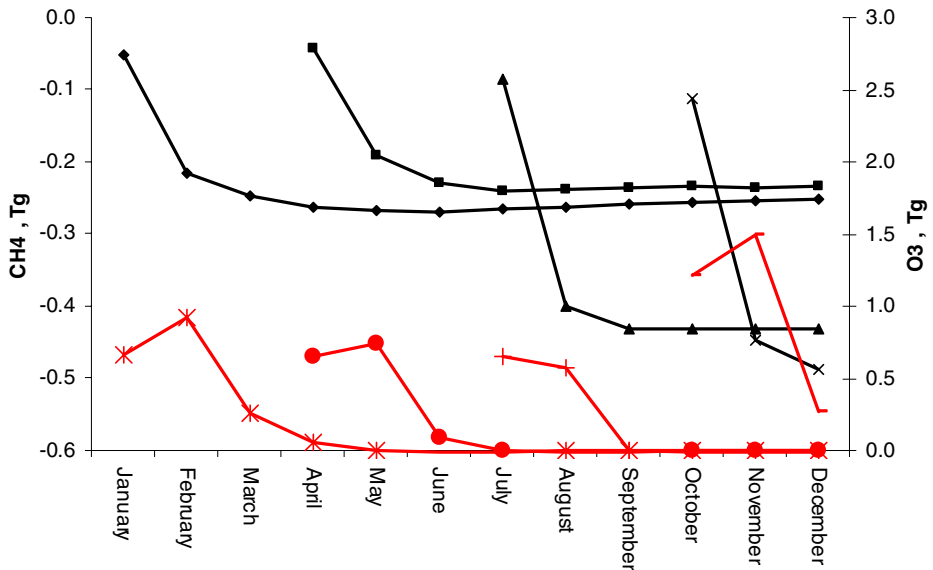


Fig. 1 Time variations in the excess CH_4 (black lines) and O_3 (red lines) burdens over the period from 1st January to 31st December following NO_x emission pulses of 0.2 Tg N per month emitted during January, April, July and October centred over Japan

Table 1 presents the time-integrated perturbations in the global burdens of CH₄ and O₃ following the emission of NO_x pulses in North America, Europe and Asia during January. The time-integrated CH₄ perturbations spanned a factor of about five across the three cases, with European NO_x emission pulses showing the least response and Asian emission pulses the greatest response. The sum of the long-term and short-term O₃ responses spanned a much narrower range with North American emission pulses giving the largest response and the European pulses the least. These results are broadly in line with the results presented by Fuglestedt et al. (1999), Bernsten et al. (2005) and Naik et al. (2005), though the relative O₃ responses between Europe and Asia are much smaller here and are discussed further in Section 5 below. In all these cases, and in those discussed below, the spatial scales of the long-lived CH₄ and short-lived O₃ perturbations were markedly different. The CH₄ perturbation was global in extent whilst the O₃ perturbation was localized to the region of the pulse and that immediately downwind.

4.2 Regional-scale NO_x emission pulses: variation with sign and magnitude

In a second series of transient experiments, the linearities of the CH₄ and O₃ responses to the size and sign of NO_x emission pulses were checked. In each model experiment summarized in Table 2, the NO_x emission pulse was applied during January and over an area of 10° longitude × 10° latitude centred over Japan. Experiments were performed with both negative emission pulses, where the NO_x emissions in the 4 STOCHEM 5° × 5° emission chosen grid squares were reduced below their base case values and with positive pulses as in Section 4.1 above. The magnitudes of the pulses and the absolute NO_x emissions achieved in each experiment are given in Table 2. In the experiments with negative pulses, the responses of the CH₄ and O₃ global burdens were exactly analogous to those with positive pulses, except with opposite signs.

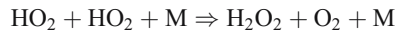
Table 2 presents the time-integrated CH₄ and O₃ responses, normalised to a positive 1 Tg(NO₂) emission pulse. These all showed consistent trends throughout the series of experiments, irrespective of the sign of the emission pulses. Normalised CH₄ and O₃ responses both steadily increased in magnitude with decreasing grid square emissions of NO_x. If the normalized responses had been independent of pulse size, the system would have been behaving linearly. Since this was not the case, the system showed some degree of non-linearity. The modelled CH₄ and O₃ responses became relatively more sensitive as the total NO_x emissions for the grid square reduced. The origin of the non-linearity in the OH and HO₂ number densities and hence CH₄ and O₃ responses at low NO_x levels was found to

Table 1 Time-integrated global methane and ozone responses to NO_x emission pulses applied to different regions during January and normalized to the basis of 1 Tg NO₂

Geographical region	Latitude range	Longitude range	Time-integrated CH ₄ response (ppb years)	Time-integrated O ₃ response (ppb years)	Time-integrated O ₃ response (ppb years)
				Short term	Long-term
North America	10°–50°N	130°–50°W	–2.0	0.026	–0.008
Europe	30°–70°N	10°W–70°E	–0.6	0.013	–0.002
Asia	0°–40°N	60°–140°E	–3.1	0.027	–0.012

All experiments were normalized to a NO_x emission pulse of 1 Tg NO₂. Time integrations were performed over a 100-year time horizon.

be due to the competition between the following first order and second order radical loss processes as originally suggested by Lin et al. (1988):



The competition between these processes introduces non-linearities since the first is a removal process for HO_x ($=\text{OH}+\text{HO}_2$) radicals whereas the second is a removal process for both HO_x and NO_x .

However, the net time-integrated radiative forcing RF, which is the linear combination of the forcings from CH_4 and the short-term and long-term O_3 components, shows a partial cancellation between terms, and has a peak value for small positive pulse sizes in this case. Hence, the calculated GWP from a given simulation shows some dependence on the pulse size; here for a range of pulse sizes varying by a factor of 32 in magnitude, and also in sign, we find GWPs in the range -3.5 to -5.2 , i.e. a spread of $\pm 20\%$ around a central value. This represents a typical uncertainty in GWP due to experimental design, although of course, in percentage terms the range may be much wider if the individual terms cancel and produce GWPs closer to zero. For the rest of this study, we use emission pulses of fixed magnitude of 0.2 Tg(N) (0.66 Tg NO_2), and to maintain consistency with previous work, linearly scale our results to emission pulse sizes of $1 \text{ Tg(NO}_2)$, even though we know that this linearity is an approximation.

4.3 Regional-scale NO_x emission pulses: variation with season

In a third series of experiments, the time period of the 0.2-Tg N per month emission pulse centred over Japan was shifted from January to April, July and October. The responses of the global CH_4 and O_3 burdens are shown in Fig. 1 and are qualitatively the same irrespective of the season in which the pulse was applied. In all experiments, the CH_4

Table 2 Normalised time-integrated responses of methane and ozone, net radiative forcing, and GWPs for surface NO_x emission pulses of varying signs and magnitudes applied to the region centred over Japan during January

NO_x emission pulse $\text{Tg(N)}/\text{month}$	Normalised time-integrated CH_4 response ppb year	Normalised time-integrated short-term O_3 response ppb year	Normalised time-integrated long-term O_3 response ppb year	Normalised net time-integrated radiative forcing $\text{mW m}^{-2} \text{ year}$	GWP
0.20	-1.91	0.035	-0.007	-0.37	-3.5
0.10	-2.19	0.040	-0.008	-0.42	-4.0
0.05	-2.43	0.044	-0.009	-0.47	-4.5
0.025	-2.58	0.046	-0.010	-0.51	-4.8
0.0062	-2.66	0.049	-0.010	-0.55	-5.2
-0.0062	-2.74	0.055	-0.011	-0.48	-4.6
-0.012	-2.79	0.058	-0.011	-0.46	-4.4
-0.019	-2.93	0.062	-0.011	-0.48	-4.6

Responses are normalized to a pulse magnitude of $+1 \text{ Tg(NO}_2)$. Regions: $30^\circ\text{--}40^\circ\text{N}$, $130^\circ\text{--}140^\circ\text{E}$. Baseline man-made NO_x emissions for this region are $0.055 \text{ Tg(N)}/\text{month}$. Integrations were performed over a 100-year time horizon. GWPs are calculated for a 100-year time horizon. AGWP for the CO_2 reference gas is taken to be $0.81 \text{ W m}^{-2} \text{ years ppm}^{-1}$.

deficits peaked between 3 and 6 months after the initiation of the pulse and the O₃ excesses peaked during the month of the pulse or the month after.

However, there were differences in detail between the CH₄ and O₃ responses between the different seasonal experiments. CH₄ deficits were largest for pulses emitted in October and smallest for April. O₃ excesses were largest for pulse emitted in October and smallest for July. The season of emissions is therefore an important determinant of the responses of the global CH₄ and O₃ burdens to NO_x emission pulses arising from the Asian continent. Stevenson et al. (2004) also found variations in the response of the STOCHEM model to pulses of NO_x emissions, although in that case the emissions were from aircraft mainly into the upper troposphere. For aircraft NO_x, the CH₄ was most responsive in July and least in October, whilst O₃ was most sensitive to emissions in April and least in July. This suggests that the seasonality in the responses are generally different if the emissions are in the upper troposphere rather than at the surface. The seasonality can be interpreted in terms of a complex combination of competing factors, including (1) the efficiency of O₃ production, which peaks in the summer, (2) O₃ destruction which is least effective in the winter, (3) the production of OH from the excess NO_x and O₃ which peaks in the summer, and (4) the oxidation of CH₄ by OH which also peaks in the summer. To eliminate any complications arising from seasonality, the remaining model experiments have therefore standardized on January emission pulses of 0.2 Tg N per month.

4.4 Radiative forcing from Asian NO_x emissions: influence of location

In the final set of model experiments, we emitted pulses from 21 different source locations widely spread across Asia, in each case adding an additional 0.2 Tg N of NO_x to a 10°×10° area, see Table 3 for the chosen locations, in January. With this pulse size, NO_x emission densities were raised by a considerable factor over and above those in the base case experiment. For example, in the case of the 10°×10° grid square centred over Japan, NO_x emission densities were raised by a factor of 4.6; other regions experienced even larger fractional increases. These clearly were large perturbations that represented a compromise between producing CH₄ and O₃ responses that were not lost in the noise of our coupled chemistry–climate modelling system nor produced gross and unrealistic distortions in the model chemistry. The linearity of the model responses has been treated in some detail above. Nevertheless, the magnitudes of the pulses may have implications for the comparison of our results with previous studies, see Section 5 below.

Table 3 shows the time-integrated perturbations to the global mean mixing ratios (over the whole model domain, i.e. surface to 100 hPa) of CH₄ and O₃ that resulted from equal mass NO_x pulses emitted in the different regions. Time-integrated CH₄ mixing ratio responses varied by a factor of about 6 from about −0.9 ppb years when the pulse was emitted over the northern part of India to about −6 ppb years when emitted over Java and Sumatra, normalized to a NO_x emission pulse of 1 Tg NO₂. The range of these regional responses encompasses the CH₄ response of −3 ppb years found in the Asian continental pulse experiment reported in Table 1.

As described in Section 4.1, NO_x emissions can increase the OH concentrations, either directly, by converting HO₂ into OH, or indirectly, by forming ozone which can be photolysed in the presence of water vapour to produce OH. Several spatial factors appeared to be at work in the results in Table 3. CH₄ responses became dramatically more negative towards the southerly regions of Asia with a reduction of more than −2 ppb years being reported for the Philippines, Malaysia, Borneo and Java. CH₄ is oxidized preferentially in the tropics due to the higher temperatures, humidity and insolation found there. NO_x

Table 3 Time-integrated global methane and ozone mixing ratio responses to NO_x emission pulses applied to different regions of Asia during January

Geographical region of NO _x emission pulse	Latitude range (°N)	Longitude range (°E)	Time-integrated CH ₄ response (ppb years)	Time-integrated O ₃ response (ppb years)	
				Short-term	Long-term
Afghanistan	30–40°	60–70°	-1.29	0.034	-0.005
Kashmir		70–80°	-1.31	0.031	-0.005
China 1		80–90°	-1.90	0.037	-0.007
China 2		90–100°	-1.77	0.034	-0.007
China 3		100–110°	-1.26	0.025	-0.005
China 4		110–120°	-1.09	0.020	-0.004
Korea		120–130°	-1.45	0.024	-0.006
Japan		130–140°	-1.91	0.035	-0.007
Pakistan	20–30°	60–70°	-1.48	0.023	-0.006
India 2		70–80°	-0.96	0.011	-0.004
India 1		80–90°	-0.95	0.015	-0.004
Myanmar		90–100°	-1.08	0.020	-0.004
China 5		100–110°	-0.96	0.019	-0.004
China 6		110–120°	-1.04	0.016	-0.004
India 3	10–20°	70–80°	-1.68	0.010	-0.006
Thailand 2		90–100°	-1.74	0.010	-0.007
Thailand 1		100–110°	-1.93	0.015	-0.007
Philippines		130–140°	-2.62	0.020	-0.010
Malaysia	0–10°	100–110°	-4.21	0.030	-0.016
Borneo		110–120°	-3.76	0.025	-0.015
Java	-10° to 0°	100–110°	-6.10	0.033	-0.024

All experiments were normalized to a NO_x emission pulse of 1 Tg NO₂. Long-term phases were calculated over a 100-year time horizon by extrapolation using the CH₄ adjustment time of 11.53 years following Stevenson et al. (2004).

emissions at lower latitudes therefore have a greater effect on CH₄ destruction there. There was a local maximum of about 1.9 ppb years in the CH₄ decrease that appeared to be associated with the Himalaya Mountains and the Tibetan Plateau in the most northerly part of the region studied (see Table 3 entries for China 1 and 2). NO_x emissions in this region generate large ozone responses (see below) which are likely to have been responsible for the additional CH₄ decreases. A further maximum CH₄ decrease with a similar magnitude of about 1.9 ppb years was also associated with Asian outflow into the Pacific region over Japan. This again is expected to be due to the greater ozone production from these emissions.

Stevenson et al. (2004) showed that the response of CH₄ and O₃ to aircraft NO_x emissions was the result of a complex balance between competing reactions associated with O₃ and OH production. In addition to seasonal variations, these reactions also have strong spatial (latitude and altitude) variations, due to variations in climate and background levels of emissions; these strongly influence the geographical response to NO_x emissions in the results presented here for surface sources.

The sum of the short-term and long-term time-integrated O₃ mixing ratio responses varied by about an order of magnitude depending on whether the NO_x pulse was emitted in southern India or Thailand or in the more northerly areas of Afghanistan, Eastern China and Japan. This range encompasses the response found in the Asian continent experiment reported in Table 1. Spatial factors were much more complicated in the case of the O₃

responses compared with the CH₄ responses because there were spatial factors working on both the short-term NO_x-driven initial phase and on the long-term CH₄-driven phase. The short-term initial phase showed maxima in the extreme north and in the tropical areas of the south, with a minimum in southern India and Thailand. This phase is driven by direct photochemical production of ozone by NO_x. As described in Section 4.3, this production is more efficient in regions of higher insolation and lower background NO_x. Therefore emissions into, or rapidly transported to, such regions give larger short-term responses. In our study, the equatorial emissions (Malaysia, Java, Borneo) were into high insolation, low background NO_x regions and efficiently produced ozone. Emissions from the Japanese region were quickly advected into the low-NO_x environment of the Pacific, giving them an increased ozone production efficiency. Emissions from India, Eastern China and Thailand were into an already polluted background and so produced less additional O₃. The reasons for the efficient production over the Himalaya and Tibetan plateau (Afghanistan, Kashmir, China 1 and 2) have not been examined in detail but are likely to be due to the emissions being at higher altitude into a cleaner background and to transport pathways associated with the elevated orography.

The long-term O₃ response was determined by scaling the CH₄ response and hence was negative throughout. It was small through much of the study region but was larger (following the CH₄ response) over the Philippines, Malaysia, Borneo and Java. The sum of the short-term and long-term time integrated O₃ responses were therefore strongly influenced by the Himalaya Mountains and Asian outflow in the more northerly areas and by the proximity of the tropics in the more southerly areas.

The short-term initial NO_x-driven phase and the long-term CH₄-driven phase time- and globally-integrated O₃ RFs are given in Table 4, together with the total net RF of the CH₄ and two O₃ forcing terms, assuming complete additivity of the global mean RFs. Because the time-integrated CH₄ RFs and those of the short-term initial NO_x-driven phase O₃ terms were roughly of the same order of magnitude but different signs, (CH₄ cooling and O₃ warming), there is a great deal of cancellation when the total net time-integrated RFs are calculated, see Table 4. Total net time-integrated RFs varied through a range of a factor of 15 from -0.11 to -1.7 mW m⁻² years for NO_x emission pulses applied in Afghanistan and Java, respectively. Although there is a great deal of cancellation in the global total net time-integrated RF, there will still be significant spatial variations in the net RFs because of the different spatial scales of the CH₄ and O₃ components.

Geographical influences are evident in the radiative forcing consequences of the NO_x emission pulses emitted in different Asian regions. This is illustrated in Fig. 2 by showing the magnitudes of the different globally-integrated RFs as a tile map using the location of the respective emission pulses. So, for example, the coloured tile over Java (upper left panel, Fig. 2) represents the largest negative globally-integrated CH₄ response to any of the regional NO_x pulses, when integrated over 100 years time horizon. The pulse emitted over Java gave a radiative forcing of -2.3 mW m⁻² years found by integrating the CH₄ mixing ratio responses throughout the globe. The smallest negative CH₄ response of -0.35 mW m⁻² years was thus found from the NO_x emission pulse emitted over India. The upper right hand panel shows the globally-integrated RF from the short-term O₃ responses. These responses peaked at 1.0 mW m⁻² years with the pulse emitted over Java and were at a minimum with the pulse emitted over India. The long-term O₃ map (lower left panel, Fig. 2) followed that of CH₄ because of the constant 0.23 scaling factor chosen. NO_x emission pulses emitted over Java gave the largest negative total RF (lower right panel, Fig. 2) of -1.7 mW m⁻² years and those emitted over Afghanistan, the least negative total. Features in these maps could be identified showing evidence of the influence from the tropical warm-pool over Indonesia,

Table 4 Time-integrated global methane and ozone radiative forcing responses to NO_x emission pulses applied to different regions of Asia during January

Geographical region of NO _x emission	Time-integrated CH ₄ response (mW m ⁻² years)	Time-integrated O ₃ response (mW m ⁻² years)		Total net response (mW m ⁻² years)	GWP
		Short term	Long term		
Afghanistan	-0.48	0.48	-0.11	-0.11	-1.0
Kashmir	-0.48	0.45	-0.11	-0.15	-1.4
China 1	-0.70	0.53	-0.16	-0.33	-3.2
China 2	-0.65	0.49	-0.15	-0.31	-3.0
China 3	-0.47	0.38	-0.11	-0.20	-1.9
China 4	-0.40	0.31	-0.093	-0.18	-1.7
Korea	-0.54	0.36	-0.12	-0.30	-2.8
Japan	-0.71	0.51	-0.16	-0.37	-3.5
Pakistan	-0.55	0.37	-0.13	-0.31	-2.9
India 2	-0.35	0.18	-0.081	-0.25	-2.4
India 1	-0.35	0.25	-0.080	-0.18	-1.7
Myanmar	-0.40	0.29	-0.092	-0.21	-2.0
China 5	-0.36	0.28	-0.082	-0.16	-1.5
China 6	-0.39	0.28	-0.089	-0.20	-1.9
India 3	-0.62	0.22	-0.14	-0.54	-5.2
Thailand 2	-0.65	0.21	-0.15	-0.59	-5.6
Thailand 1	-0.72	0.25	-0.16	-0.63	-6.0
Philippines	-0.97	0.40	-0.22	-0.79	-7.5
Malaysia	-1.56	0.89	-0.36	-1.02	-9.7
Borneo	-1.39	0.69	-0.32	-1.02	-9.7
Java	-2.26	1.05	-0.52	-1.73	-16.5

Time integrations are performed over a 100-year time horizon. The latitude and longitude ranges of the geographical regions are given in Table 3. GWPs are calculated for a 100-year time horizon and on the basis of 1 Tg NO₂. AGWP for the CO₂ reference gas is taken to be 0.81 W m⁻² years ppm⁻¹.

Asian outflow over Japan and Korea and of the Himalayas on the global RF consequences of NO_x emission pulses emitted over different regions of Asia as revealed in the different panels in Fig. 2.

4.5 Global warming potentials for surface NO_x emissions emitted over Asia

In our previous studies of GWPs (Derwent et al. 2001), we have determined that a pulse of 1 Tg of carbon dioxide CO₂ added to the atmosphere decays away and generates an additional time-integrated burden of 5.976 ppb years over a 100-year time horizon using the CO₂ response function of the Bern carbon cycle model (IPCC 1995) run for a constant mixing ratio of CO₂ over a 500-year period. Using a radiative efficiency of 1.75×10^{-5} W m⁻² ppb⁻¹ (IPCC 1996), then the instantaneous emission of 1 Tg of CO₂ leads to the absolute global warming potential AGWP of 1.05×10^{-4} W m⁻² years over a time horizon of 100 years. By dividing the total time-integrated RFs in Table 4 by the AGWP of the reference gas CO₂, the column of GWPs were obtained for a 100-year time horizon. The AGWP for CO₂ employed here is equivalent to 0.81 W m⁻² years ppm⁻¹ which is close to the 0.800-W m⁻² years ppm⁻¹ value recommended by WMO (1999).

GWPs for surface NO_x emissions over a 100-year time horizon thus varied from -1.0 to -16.5 over the Asian regions studied from Afghanistan to Java, respectively. This range

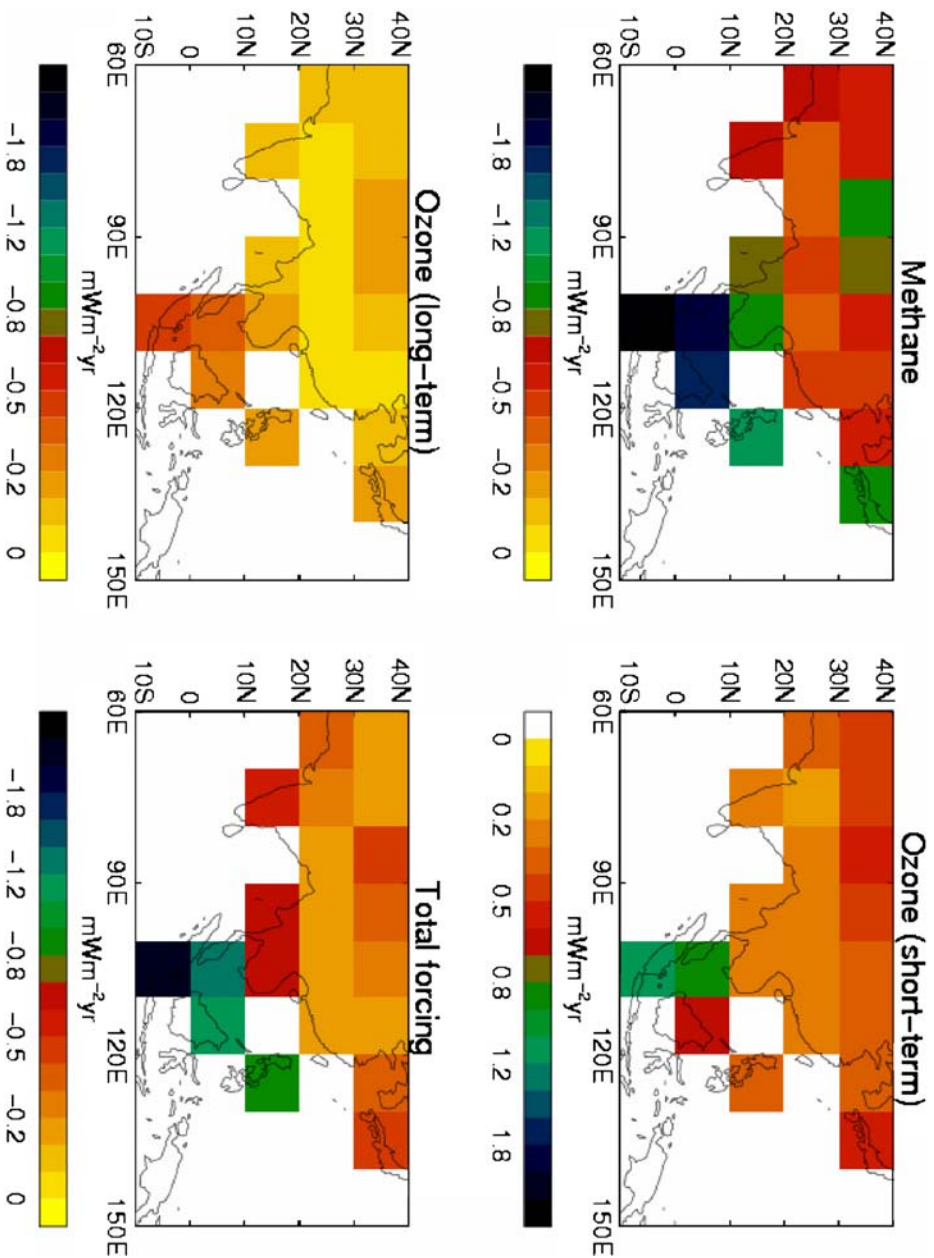


Fig. 2 Contributions from methane and ozone (both short-term and long-term) to and the total globally-integrated radiative forcing in $\text{mW m}^{-2} \text{ yr}^{-1}$ from pulses of 1 Tg NO_2 emitted in January from each particular region of Asia

encompasses the GWP of -8 calculated for the entire Asian region from the experiments in Table 1. The corresponding GWPs for North America and Europe were -4 and -0.7 , respectively.

5 Discussion of the results

The time-integrated RFs and GWPs reported here are first compared with our previous work. Stevenson et al. (2004) have noted that the estimates in Derwent et al. (2001) were incorrectly normalized to 1 Tg NO_2 and those in Derwent et al. (2001, 2002) neglected the long-term CH_4 -driven phase of the ozone radiative forcing and so failed to include a significant negative (cooling) term. Making these corrections, our previous work gave a RF of $-0.53 \text{ mW m}^{-2} \text{ years}$ (GWP -5.0) for a northern hemisphere surface NO_x emission pulse of 1 Tg NO_2 . The estimates in Table 4 span the range from -0.1 to $1.7 \text{ mW m}^{-2} \text{ years}$ with an average of $-0.46 \text{ mW m}^{-2} \text{ years}$ (GWP -4.4), in agreement with our previous work. The corrections to our previous work give $-1.78 \text{ mW m}^{-2} \text{ years}$ (GWP -17.2) for a corresponding southern hemisphere NO_x source in agreement with the $-2.0 \text{ mW m}^{-2} \text{ years}$ (GWP -19.0) estimated for Java, the most southerly region studied here.

We conclude that our studies confirm that both the time-integrated RFs and GWPs for surface NO_x sources are all negative (climate cooling), despite showing large variability with location, for a 100-year time horizon. This sign implies that the magnitude of the RF from the surface NO_x -driven CH_4 depletion tends to approach and outweigh that from the O_3 enhancement. This is in contrast with the corresponding situation for aircraft NO_x emissions. In this case, the RF from aircraft NO_x -driven O_3 enhancement largely outweighs that from CH_4 depletion giving RFs and GWPs that are positive (climate warming) or close to zero based on $-0.09 \text{ mW m}^{-2} \text{ years}$ per 1 Tg NO_2 from Stevenson et al. (2004), $+3.3 \text{ mW m}^{-2} \text{ years}$ (corrected: Derwent et al. 2002) and $+1.8 \text{ mW m}^{-2} \text{ years}$ (Wild et al. 2001). This reversal in the signs of the RFs between surface and aircraft NO_x sources in some studies reflects the greater efficiency of photochemical O_3 production compared with CH_4 destruction in the upper troposphere compared with the surface.

Much of the literature addressing RF from surface NO_x sources uses step changes or sustained emission reductions and the results described are not directly comparable with those from the pulse emission experiments carried out here. In principle, since a step change can be represented by a series of pulses, it should be possible to extrapolate the results from our pulse experiments to the step change situation. There are, however, difficulties with these extrapolations if the system exhibits non-linearities. Extrapolating from our January continental-scale pulse experiments (Table 1) to the step change experiments of Naik et al. (2005), we estimate that our short-lived $\Delta\text{O}_3/\Delta\text{ENO}_x$ sensitivities range are 0.38 (Asia), 0.45 (N. America), and 0.28 (Europe); these compare to Naik et al. (2005): 0.32 (E. Asia), 0.29 (N. America), and 0.05 (Europe). Our definition of Asia is larger than Naik's E. Asia, and includes their India and S.E. Asia, which have higher values. Our estimate for Asia of $0.68 \text{ Tg O}_3/\text{Tg N year}^{-1}$ is significantly less than those for India ($0.99 \text{ Tg O}_3/\text{Tg N year}^{-1}$) and south east Asia ($2.70 \text{ Tg O}_3/\text{Tg N year}^{-1}$) from Naik et al. (2005). In contrast, our estimate for Europe is significantly greater than that from Naik et al. (2005). It may well be that these comparisons could be improved if we took seasonal variations into account in our extrapolation to the step change case. Fuglestedt et al. (1999) gave O_3 RF sensitivities of 2.9, 3.5 and 23.7 mW m^{-2} per Tg N year^{-1} , respectively, for Scandinavia, USA and south east Asia (Naik et al. Table 2 has equivalent: 0.06, 1.2, and 21, for Europe, N. America, and S.E. Asia, respectively).

Extrapolating from our January continental pulse experiments, the corresponding sensitivities found here are 0.5, 1.1, 1.0 mW m^{-2} per Tg N year^{-1} . The present estimates are roughly of a similar magnitude to the Fuglestedt et al. (1999) values for Europe and North America but are significantly smaller for south east Asia. This may reflect the magnitude of the emission pulses employed in this study.

The CH_4 sensitivities $\Delta\text{CH}_4/\Delta\text{NO}_x$ reported by Naik et al. (2005) range from -3.2 through -6.8 to -16 and -46 $\text{ppb/Tg N year}^{-1}$, for Europe, North America, India and S.E. Asia, respectively. Extrapolation from the results reported here generates comparable sensitivities of -2.0 , -6.6 , -3.9 (average of our three Indian regions) and -11 (average of six regions: Malaysia, Philippines, Thailand 1 and 2, Borneo and Java) $\text{ppb CH}_4/\text{Tg N year}^{-1}$ based on January NO_x emission pulses. The present results agree well over N. America, but estimate lower sensitivities for Europe and significantly lower for Asia compared to those reported by Naik et al. (2005). It may be the lack of seasonal treatment with our continental pulse experiments is disguising what looks to be reasonable agreement, despite the wide differences in the model experimental designs. Fuglestedt et al. (1999) report CH_4 RF sensitivities of -3.7 , -5.0 and -23.2 mW m^{-2} per Tg N year^{-1} that are significantly larger than the estimates of -0.7 , -2.4 and -3.8 mW m^{-2} per Tg N year^{-1} extrapolated here for Europe, North America and Asia, respectively. Despite these differences, the work presented here and by Fuglestedt et al. (1999) and by Naik et al. (2005) confirm that the location of the NO_x emission source is an important determinant of the RF terms and that the net RFs increase from Europe, through North America to Asia. The magnitude and structure of both the short-lived initial O_3 and subsequent long-lived CH_4 and O_3 perturbations in response to changes in NO_x emissions are strongly controlled by the model representations of chemistry, transport and mixing. Direct comparison of these different studies is rendered difficult, partly because of differences in our experimental approaches. Further work with a variety of models is required to increase confidence in the quantification of these responses. A model intercomparison with all models using the same methods would be a useful approach to further understand how consistent models are for this key policy area.

In addition to the variations between the continents, the present study has shown that the time-integrated RFs and GWPs of surface NO_x sources show important variations with emission size, season and location within a particular chosen continent, Asia. These seasonal variations appear to be linked to seasonal changes in the OH-driven CH_4 oxidation rate and those in emission size to the competition between HO_2 radicals for NO and HO_2 and between OH radicals for NO_2 . Variations with location appear to be driven by latitude, with background NO_x concentrations and efficiency of transport (both horizontal and vertical) also important as discussed in Section 4.4 above. Whilst all of these factors are treated with some level of confidence in STOCHEM, the representation of the underlying processes is highly model-dependent and there are currently no standard representations against which the descriptions in STOCHEM can be evaluated. If the spatial, seasonal and pulse size variations identified in this study turn out to reflect real behaviour in the troposphere, then we must conclude that there is no simple robust relationship between continental-scale NO_x emissions and globally-integrated radiative forcing and this will contribute to uncertainty and hesitancy on the part of policymakers.

Despite these variations, all of our model experiments demonstrate that pulses of surface NO_x lead to negative radiative forcing (climate cooling) supporting the results of previous studies (Fuglestedt et al. 1999; Wild and Prather 2000; Derwent et al. 2001). The corollary is that control of man-made surface NO_x emissions alone will inevitably lead to positive radiative forcing (climate warming). It should be acknowledged that in the real world,

control of NO_x is likely to be accompanied by controls of other O₃ precursor emissions, notably CO and VOCs, and their combined effects will be important. In view of the dependence of the RFs and GWPs for surface NO_x emissions on pulse size, season and location, it is concluded that many more studies will be required before a robust assessment can be completed of the RFs and GWPs for NO_x. In addition, the impact of NO_x emissions on climate through the formation of nitrate aerosol should also be taken into account (Schaap et al., 2004; Liao and Seinfeld 2005). Furthermore, there are potential indirect climate impacts of NO_x deposition through interaction with the global carbon cycle (Schimel 1995). Without the inclusion of NO_x in the United Nations Framework Convention on Climate Change, it is difficult to see how future levels of methane and tropospheric ozone can be stabilized and eventually reduced to combat global climate change.

Acknowledgements This study was sponsored by the Air and Environmental Quality Division of the United Kingdom Department for Environment, Food and Rural Affairs through contract CPEA 7, by the GMR Programme of the Met Office and by a NERC/Environment Agency Advanced Fellowship (P4-F02, NER/J/S/2000/00840) to one of us (DSS).

References

- Berntsen T, Fuglestedt J, Joshi MM, Shine KP, Stuber N, Ponater M, Sausen R, Hauglustaine DA, Li L (2005) Response of climate to regional emissions of ozone precursors: sensitivities and warming potentials. *Tellus* 57B:283–304
- Berntsen T, Fuglestedt J, Myhre G, Stordal F, Berglen TF (2006) Abatement of greenhouse gases: does location matter? *Clim Change* 74:377–411
- Cofala J, Amann M, Klimont Z, Kispiosnen K (2005) Scenarios of global anthropogenic emissions of air pollutants and methane up to 2030. International Institute for Applied Systems Analysis, Laxenburg, Austria
- Collins WJ, Stevenson DS, Johnson CE, Derwent RG (1997) Tropospheric ozone in a global-scale three-dimensional Lagrangian model and its response to NO_x emission controls. *J Atmos Chem* 26:223–274
- Collins WJ, Derwent RG, Johnson CE, Stevenson DS (2002) The oxidation of organic compounds and their global warming potentials. *Clim Change* 52:453–479
- Dentener F, Stevenson D, Cofala J, Mechler R, Amann M, Bergamaschi P, Raes F, Derwent R (2005) The impact of air pollutant and methane emission controls on tropospheric ozone and radiative forcing: CTM calculations for the period 1990–2030. *Atmos Chem Phys* 5:1731–1755
- Derwent RG, Collins WJ, Johnson CE, Stevenson DS (2001) Transient behaviour of tropospheric ozone precursors in a global 3-D CTM and their indirect greenhouse effects. *Clim Change* 49:463–487
- Derwent RG, Collins WJ, Johnson CE, Stevenson DS (2002) Global warming potentials for non-CO₂ greenhouse gases. In: van Ham J, Baede APM, Guicherit R, Williams-Jacobse JGFM (eds) *Non-CO₂ greenhouse gases*. Millpress, Rotterdam, The Netherlands
- Edwards JM, Slingo A (1996) Studies with a flexible new radiation code. I. Choosing a configuration for a large-scale model. *Q J R Meteorol Soc* 122:689–719
- Fuglestedt JS, Isaksen ISA, Wang W-C (1996) Estimates of indirect global warming potential for CH₄, CO and NO_x. *Clim Change* 34:404–437
- Fuglestedt JS, Berntsen TK, Isaksen ISA, Mao H, Liang X-Z, Wang W-C (1999) Climatic effects of NO_x emissions through changes in tropospheric ozone and methane; global 3-D model studies. *Atmos Environ* 33:961–977
- Fuglestedt JS, Berntsen TK, Godal O, Sausen R, Shine KP, Skodvin T (2003) Metrics of climate change: assessing radiative forcing and emission indices. *Clim Change* 58:267–331
- Godal O, Fuglestedt JS (2002) Testing 100-year global warming potentials: impacts on compliance costs and abatement profile. *Clim Change* 52:93–127

- Hansen J, Sato M, Ruedy R, Nazarenko L, Lacis A, Schmidt GA, Russell G, Aleinov I, Bauer M, Bauer S, Bell N, Cairns B, Canuto V, Chandler M, Chemng Y, Del Gonio A, Faluvegi G, Fleming E, Friend A, Hall T, Jackman C, Kelley M, Kiang M, Kiang N, Koch D, Lean J, Lerner J, Lo K, Menon S, Miller R, Minnis P, Novakov T, Oinas V, Perlwitz Ja, Perlwitz Ju, Rind D, Romanou A, Shindell D, Stone P, Sun S, Tausnev N, Thresher D, Wielicki B, Wong T, Yao M, Zhang S (2005) Efficacy of climate forcings. *J Geophys Res* 110:D18104, DOI [10.1029/2005JD005776](https://doi.org/10.1029/2005JD005776)
- IPCC (1990) *Climate change 1990: the scientific basis*. Cambridge University Press, New York
- IPCC (1995) *Climate change 1994*. Cambridge University Press, New York
- IPCC (1996) *Climate change 1995: the scientific basis*. Cambridge University Press, New York
- IPCC (1999) *IPCC special report on aviation and the global atmosphere*. Cambridge University Press, New York
- IPCC (2001) *Climate change 2001: the scientific basis*. Cambridge University Press, New York
- Joshi MM, Shine KP, Ponater M, Stuber M, Sausen R, Li L (2003) A comparison of climate response to different radiative forcings in three general circulation models: towards an improved estimate of climate change. *Clim Dyn* 20:843–854
- Li D, Shine K (1995) A 4-dimensional ozone climatology for UGAMP models. UK Universities Global Atmospheric Modelling Programme. Internal Report, University of Reading, UK
- Liao H, Seinfeld JH (2005) Global impacts of gas-phase chemistry-aerosol interactions on direct radiative forcing by anthropogenic aerosols and ozone. *J Geophys Res* 110:D18208, DOI [10.1029/2005JD005907](https://doi.org/10.1029/2005JD005907)
- Lin X, Trainer M, Liu SC (1988) On the non-linearity of the tropospheric ozone production. *J Geophys Res* 93:15879–15888
- Murphy DM, Fahey DW (1994) An estimate of the flux of stratospheric reactive nitrogen and ozone into the troposphere. *J Geophys Res* 99:5325–5332
- Naik V, Mauzerall D, Horowitz L, Schwarzkopf MD, Ramaswamy V, Oppenheimer M (2005) Net radiative forcing due to changes in regional emissions of tropospheric ozone precursors. *J Geophys Res* 110: D24306, DOI [10.1029/2005JD005908](https://doi.org/10.1029/2005JD005908)
- Olivier JGJ, Berdowski JJM (2001) Global emissions sources and sinks. In: Berdowski JJM, Guicherit R, Heij BJ (eds) *The climate system*. Swets & Zeitlinger, Lisse, The Netherlands
- Schaap M, van Loon M, ten Brink HM, Dentener FJ, Builtjes PJH (2004) Secondary inorganic aerosol simulations for Europe with special attention to nitrate. *Atmos Chem Phys* 4:857–874
- Schimel DS (1995) Terrestrial ecosystems and the carbon cycle. *Glob Chang Biol* 1:77–91
- Schimel, D et al. (1996) Radiative forcing of climate change. In: Houghton JT, Meira Filho LG, Callander BA, Harris N, Kattenburg A, Maskell K (eds) *Climate change 1995: the scientific basis*. Cambridge University Press, New York
- Shine KP, Cook J, Highwood EJ, Joshi MM (2003) An alternative to radiative forcing for estimating the relative importance of climate change mechanisms. *Geophys Res Lett* 30:2047, DOI [10.1029/2003GL018141](https://doi.org/10.1029/2003GL018141)
- Shine KP, Fuglestedt JS, Hailemariam K, Stuber N (2005a) Alternatives to the global warming potential for comparing climate impacts of emissions of greenhouse gases. *Clim Change* 68:281–302
- Shine KP, Bernsten TK, Fuglestedt JS, Sausen R (2005b) Scientific issues in the design of metrics for inclusion of oxides of nitrogen in global climate agreements. *Proc Natl Acad Sci* 102:15768–15773
- Stevenson DS, Johnson CE, Collins WJ, Derwent RG, Shine KP, Edwards JM (1998) Evolution of tropospheric ozone radiative forcing. *Geophys Res Lett* 25:3819–3822
- Stevenson DS, Doherty RM, Sanderson MG, Collins WJ, Johnson CE, Derwent RG (2004) Radiative forcing from aircraft NO_x emissions: mechanisms and seasonal dependence. *J Geophys Res* 109:D17307, DOI [10.1029/2004JD004759](https://doi.org/10.1029/2004JD004759)
- Volz A, Kley D (1988) Evaluation of the Montsouris series of ozone measurements made in the nineteenth century. *Nature* 332:240–242
- Wild O, Prather MJ (2000) Excitation of the primary tropospheric chemical mode in a global three-dimensional model. *J Geophys Res* 105:24467–24660
- Wild O, Prather MJ, Akimoto H (2001) Indirect long-term global radiative cooling from NO_x emissions. *Geophys Res Lett* 28:1719–1722
- WMO (1999) *Scientific assessment of ozone depletion: 1998*. World Meteorological Organization, Global Ozone Research and Monitoring Project, Report No. 44, Geneva, Switzerland